ELSEVIER

Colloids and Surfaces
A: Physicochemical and Engineering Aspects 187–188 (2001) 493–507

COLLOIDS AND SURFACES A

www.elsevier.nl/locate/colsurfa

Self-diffusion in a fluid confined within a model nanopore structure

J.M.D. MacElroy [a,*], L.A. Pozhar [b], S.-H. Suh [c]

[a] *Department of Chemical Engineering and Conway Institute of Biomolecular and Biomedical Research, University College Dublin, Belfield, Dublin 4, Ireland*

[b] *Department of Chemical and Process Engineering, University of Surrey, Guildford, Surrey, GU2 5XH, UK*

[c] *Department of Chemical Engineering, Keimyung University, Taegu, 704-701, South Korea*

Abstract

Recent technical improvements in the molecular dynamics (MD) simulation technique have led to re-evaluation of the transport properties of fluids confined in narrow capillary pores of several molecular diameters in width (or nanofluids). Coincident with these developments, it has also become clear that unambiguous predictions of the transport properties of nanofluids may only be made when a rigorous analysis based on statistical mechanical theory is considered in conjunction with molecular simulation studies. In this paper, the theoretical analysis embodied in the Pozhar–Gubbins [L.A. Pozhar and K.E. Gubbins, J. Chem. Phys., 99 (1993) 8970; L.A. Pozhar and K.E. Gubbins, Phys. Rev., E56 (1997) 5367] statistical mechanical theory of transport in strongly inhomogeneous fluid mixtures is combined with nonequilibrium and equilibrium molecular dynamics techniques to investigate self-diffusion in a dense fluid confined within a model crystalline nanopore. The results obtained demonstrate that the spatial dependence of the transport parameters should be taken into consideration to reliably predict the diffusion fluxes within zeolitic systems. For the comparatively simple pore structure examined in this work, the local self-diffusivity varies significantly in magnitude over nanometer length scales with corresponding implications for the interpretation of the rate processes taking place within crystalline nanoporous media.

Keywords: Diffusion; Nanopores; Quasi-hydrodynamic theory; Nonequilibrium molecular dynamics

1. Introduction

Fundamental statistical mechanical analysis of the properties of fluids confined within nanopores is acquiring an increasingly important role in the design of novel adsorbents and catalyst supports. One approach which has attracted attention in the last two decades is direct molecular simulation using Monte Carlo (MC) techniques (primarily for equilibrium sorption and phase transitions) and/or molecular dynamics (MD) methods (for both transport and equilibrium properties). During this time, however, it has also become evident that future advances in this area will ultimately rely on the development of a rigorous theoretical analysis which can interrelate the microscopic

* Corresponding author. Tel.: +353-1-7061827; fax: +353-1-7061177.

E-mail address: don.macelroy@ucd.ie (J.M.D. MacElroy).

0927-7757/01/$ - see front matter
PII: S0927-7757(01)00625-2

properties of the fluid/solid system to the computational results obtained from molecular simulations. It is this interrelationship, notably in the area of diffusion transport within nanopores, which is the subject of this paper.

To date, the molecular dynamics simulation results reported for diffusion (using either equilibrium (EMD) or nonequilibrium (NEMD) methods) have been computed primarily for model pore structures subject to particular simplifying features (see for example, single pores with translational invariance or near invariance along the pore axis [3–9], random media (model silica [10–12], carbon [13–16] and polymeric systems [17–23]), or specific zeolite crystal structures [24–27]). While sharp inhomogeneities in the direction of flow have been either implicitly (EMD) or explicitly (NEMD) incorporated in a number of studies, the intrinsic influence of these inhomogeneities have not been investigated theoretically from a microscopic perspective. Here we consider NEMD simulations of diffusion of simple model nanofluids confined within a crystalline pore structure, which captures the basic geometric features of real zeolite channels interlinked by cavities. The theoretical description of diffusion in such fluids is supplied by a reduction of a general theoretical approach due to Pozhar and Gubbins (PG) [1,2]. The explicit expressions for the diffusion coefficients in the PG-theory involve the equilibrium structure factors (the fluid density and the contact values of the fluid–fluid and fluid–lattice molecule pair correlation functions) of nanoporous systems which are obtained by means of EMD simulation techniques, and a comparative analysis with the NEMD simulation results provides the basis for a mathematical model for the diffusion process suitable for engineering applications.

In Section 2, the flux equations and the mathematical details for the coefficients resulting from PG theory for self-diffusion within a nanopore fluid are presented and the MD simulation techniques employed in this work to compute the diffusion/permeation characteristics for a simple pore structure are described. In Section 3, the results of these computations are discussed and a simplified description of diffusion in nanopore fluids in terms of across-the-pore averages of the local PG-theoretical diffusion coefficients is outlined. In Section 4, we conclude the paper with a brief summary of our results.

2. Theory and simulation

2.1. Quasi-hydrodynamic theory

Intensive studies of the transport properties of nanofluids (see, for example [28–32]) resulted in a qualitative theoretical description [33,34] by Davis, and, subsequently, in the development of the rigorous, nonequilibrium statistical mechanical theory of inhomogeneous fluids [1,2] by Pozhar and Gubbins (PG). PG-theory supplies explicit expressions for the transport coefficients of inhomogeneous fluids in terms of their equilibrium structure factors (i.e. the number density and correlation functions). Recently, this theory was successfully applied to predict the viscosity of the Weeks–Chandler–Andersen (WCA) and Lennard–Jones (LJ) nanofluids confined in slit nanopores [35–37], where all other approaches including direct NEMD simulation methods fail.

In this study, we use the PG-theoretical approach to evaluate the self-diffusion coefficient of a very high pressure fluid confined within a narrow nanopore reflecting the structure and geometry of a typical pore in natural zeolites. Unfortunately, even for very high pressure bulk fluids an explicit expression for the self-diffusion coefficient has not been derived, because such a derivation involves the equation of state of the fluid which has not yet been derived rigorously from microscopic considerations even in the case of simple fluids composed of structureless molecules. For similar reasons in the case of the diffusion coefficients, PG-theory supplies only the corresponding explicit expression specific to weakly inhomogeneous fluids of moderate density. In what follows we analyse and use this expression in conjunction with the system of interest here, namely that of a high pressure fluid composed of simple nonreactive molecules which are confined within a structured zeolite-like nanopore. Similar to the conventional transport

theory of bulk fluids near equilibrium (which is a particular case of the PG-transport theory of fluids) PG-theory relies on a theoretical description of the fluid equilibrium state. In those cases, where the equilibrium thermodynamic parameters are not described theoretically, any transport theory cannot provide closed explicit expressions for all the transport coefficients. In particular, this is the case with the diffusion and thermal diffusion coefficients of very dense, strongly inhomogeneous fluids. With this in mind, we start from Eq. (4.13) of [2] in the low frequency limit which reduces significantly for the considered case of the tensorial 'tracer' self-diffusion coefficient,

$$\hat{\mathbf{D}}_{T,1*}(\mathbf{q}) = \frac{3\tau_{\mathrm{d}}(\mathbf{q})}{2\sigma^2 n_{1*}(\mathbf{q})}\sqrt{\frac{\pi\beta}{m}}\,\hat{\mathbf{D}}(\mathbf{q}), \tag{1}$$

where

$$\tau_{\mathrm{d}}^{-1}(\mathbf{q}) = \int \mathrm{d}\hat{\boldsymbol{\sigma}}\, n(\mathbf{q}-\sigma\hat{\boldsymbol{\sigma}})g(\mathbf{q},\mathbf{q}-\sigma\hat{\boldsymbol{\sigma}}) + \frac{\sqrt{2}\sigma_{\mathrm{fw}}^2}{\sigma^2}\int \mathrm{d}\hat{\boldsymbol{\sigma}}\, n_{\mathrm{w}}(\mathbf{q}-\sigma_{\mathrm{fw}}\hat{\boldsymbol{\sigma}}) \times g_{\mathrm{fw}}(\mathbf{q},\mathbf{q}-\sigma_{\mathrm{fw}}\hat{\boldsymbol{\sigma}}), \tag{2}$$

and where $\mathbf{q}$ is a position within the fluid, σ, σ_{w} and σ_{fw} are the effective diameters of the hard-core contributions to the potentials of intermolecular interactions of the fluid molecules, wall molecules, and fluid and wall molecules, respectively; $\beta = 1/k_{\mathrm{B}}T$, k_{B} is the Boltzmann constant, T is temperature, m is the mass of a fluid molecule; $n_{1*}(\mathbf{q})$, $n(\mathbf{q})$ and $n_{\mathrm{w}}(\mathbf{q})$ are the equilibrium number densities of the tracer 'component' 1*, the fluid 'mixture' and the walls, respectively; $g(\mathbf{q},\mathbf{q}-\sigma\hat{\boldsymbol{\sigma}})$ and $g_{\mathrm{fw}}(\mathbf{q},\mathbf{q}-\sigma_{\mathrm{fw}}\hat{\boldsymbol{\sigma}})$ are the contact values of the equilibrium fluid–fluid and fluid–wall pair correlation functions (PCFs), respectively, and the integrals in Eq. (2) are over the surface of the unit sphere ($\hat{\boldsymbol{\sigma}}$ is the unit vector). The Cartesian tensor $\hat{\mathbf{D}}(\mathbf{q})$ in Eq. (1) is defined from Eq. (4.9) of [2] and for the case under consideration here, can be written in the form

$$\hat{\mathbf{D}}(\mathbf{q}) = \frac{1}{\beta}[\mathbf{I} + \mathbf{F}\{n\}], \tag{3}$$

where $\mathbf{I}$ is the unit matrix and, generally, $\mathbf{F}\{n\}$ is a tensorial functional of the fluid density and composition. When the inhomogeneity of the fluid becomes large the functional $\mathbf{F}\{n\}$ no longer satisfies the equation of state specific for a moderately dense weakly inhomogeneous fluid (Eq. (4.7) of [2]); instead, the proper expression for the fluid pressure tensor is required to recover the corresponding form of this functional. At present a general equation of state applicable to the considered case of a strongly compressed and strongly inhomogeneous fluid is not available. Therefore, for the purposes of this study, we focus on the zero-order contribution to the PG-theoretical self-diffusion coefficient of Eq. (1), which corresponds to $\mathbf{F}\{n\} = \mathbf{0}$. This value is a rough approximation of the self-diffusion coefficient applicable to any fluid system whatsoever. For the system studied numerically here the average zero-order theoretical self-diffusion coefficient so determined lies within 30% of the corresponding numerical 'experimental' values found using the nonequilibrium molecular dynamics (NEMD) simulation method.

If the equilibrium temperature gradients within the nanofluid are small the number flux of the component 1*, as provided by Pozhar–Gubbins theory, can be written in terms of the PG-theoretical self-diffusion coefficient of Eq. (1), the equilibrium density of this component and the gradient of the deviation of the nonequilibrium number density of the component from its equilibrium value, $\delta n_{1*}(\mathbf{q})$,

$$\mathbf{J}_{1*}(\mathbf{q}) = -n_{1*}(\mathbf{q})\hat{\mathbf{D}}_{T,1*}(\mathbf{q}) \bullet \frac{\partial \delta n_{1*}(\mathbf{q})}{\partial \mathbf{q}} = -n_{1*}(\mathbf{q}) D_{T,1*}(\mathbf{q}) \frac{\partial \delta n_{1*}(\mathbf{q})}{\partial \mathbf{q}} \tag{4}$$

where we have incorporated the assumption $\mathbf{F}\{n\} = \mathbf{0}$ and the observation that

$$\mathbf{I} \cdot \frac{\partial \delta n_{1*}(\mathbf{q})}{\partial \mathbf{q}} = \frac{\partial \delta n_{1*}(\mathbf{q})}{\partial \mathbf{q}}$$

and where

$$D_{T,1*}(\mathbf{q}) = \frac{3\tau_{\mathrm{d}}(\mathbf{q})}{2\sigma^2 n_{1*}(\mathbf{q})}\sqrt{\frac{\pi}{m\beta}} \tag{5}$$

is the scalar, theoretical zero-order self-diffusion coefficient and the dot '•' denotes the inner product. (One should note that while Eq. (4) is similar in form to the well known Darken expres-

sion for the self-diffusion flux, there are fundamental differences involved between the Darken equation and the flux relationship provided by PG theory. The most notable of these are (i) Eq. (4) is *local* with non-local contributions appearing in the diffusivity as will be shown below and (ii) gradients of the concentration *deviations* from the equilibrium local state appear explicitly in PG theory.

From Eq. (5) and using Eq. (4.15) of [2] in the case of self-diffusion one can obtain the zero-order approximation to the phenomenological self-diffusion coefficient measurable experimentally,

$$D_{\mathrm{P}}(\mathbf{q}) = n_{1*}(\mathbf{q})D_T(\mathbf{q}) = \frac{3}{2\sigma^2}\sqrt{\frac{\pi}{m\beta}}\,\tau_{\mathrm{d}}(\mathbf{q}) = \frac{3/2\sigma^2\sqrt{\pi/m\beta}}{\left[\int \mathrm{d}\hat{\boldsymbol{\sigma}}\, n(\mathbf{q}-\sigma\hat{\boldsymbol{\sigma}})g(\mathbf{q},\mathbf{q}-\sigma\hat{\boldsymbol{\sigma}}) + \frac{\sqrt{2}\sigma_{\mathrm{fw}}^2}{\sigma^2}\int \mathrm{d}\hat{\boldsymbol{\sigma}}\, n_{\mathrm{w}}(\mathbf{q}-\sigma_{\mathrm{fw}}\hat{\boldsymbol{\sigma}})g_{\mathrm{fw}}(\mathbf{q},\mathbf{q}-\sigma_{\mathrm{fw}}\hat{\boldsymbol{\sigma}})\right]} \tag{6}$$

Introducing the notations

$$D_{\mathrm{P}}^{\mathrm{ff}}(\mathbf{q}) = \frac{3}{2\sigma^2}\sqrt{\frac{\pi}{m\beta}}\,\frac{1}{\int \mathrm{d}\hat{\boldsymbol{\sigma}}\, n(\,\mathbf{q}-\sigma\hat{\boldsymbol{\sigma}})\, g(\mathbf{q},\mathbf{q}-\sigma\hat{\boldsymbol{\sigma}})} \tag{7}$$

and

$$D_{\mathrm{P}}^{\mathrm{fw}}(\mathbf{q}) = \frac{3}{4\sigma_{\mathrm{fw}}^2}\sqrt{\frac{2\pi}{m\beta}}\,\frac{1}{\int \mathrm{d}\hat{\boldsymbol{\sigma}}\, n_{\mathrm{w}}(\mathbf{q}-\sigma_{\mathrm{fw}}\hat{\boldsymbol{\sigma}})g_{\mathrm{fw}}(\mathbf{q},\mathbf{q}-\sigma_{\mathrm{fw}}\hat{\boldsymbol{\sigma}})} \tag{8}$$

one can rewrite Eq. (6) in the familiar form

$$\frac{1}{D_{\mathrm{P}}(\mathbf{q})} = \frac{1}{D_{\mathrm{P}}^{\mathrm{ff}}(\mathbf{q})} + \frac{1}{D_{\mathrm{P}}^{\mathrm{fw}}(\mathbf{q})} \tag{9}$$

This expression conveniently represents $1/D_{\mathrm{P}}(\mathbf{q})$ as a sum of the explicit contributions, $1/D_{\mathrm{P}}^{\mathrm{ff}}(\mathbf{q})$ and $1/D_{\mathrm{P}}^{\mathrm{fw}}(\mathbf{q})$, due to fluid–fluid and fluid–wall intermolecular interactions, respectively. Of course, the fluid–fluid contribution includes the contact values of the fluid–fluid PCF which are calculated *in the presence* of the confining walls and, therefore, incorporate implicitly contributions due to the fluid–wall intermolecular interactions (or so-called excluded volume effects) as well. These implicit contributions change dramatically the fluid–fluid PCF and its contact values compared with those of the corresponding bulk fluid at the same average density and temperature (see, for example, results and discussion in [35–37]).

For convenience, all length scales reported in this work are in units of the wall atom size, σ_{w} and we define dimensionless forms for the coordinates, $\mathbf{q}^* = \mathbf{q}/\sigma_{\mathrm{w}}$, the densities, $n^*(\mathbf{q}^*) = \sigma_{\mathrm{w}}^3 n(\mathbf{q}^*)$ and $n_{\mathrm{w}}^*(\mathbf{q}^*) = \sigma_{\mathrm{w}}^3 n_{\mathrm{w}}(\mathbf{q}^*)$, and the diffusion coefficients, $D_{\mathrm{P}}^*(\mathbf{q}^*) = D_{\mathrm{P}}(\mathbf{q}^*)/D^0$, $D_{\mathrm{P}}^{\mathrm{ff}*}(\mathbf{q}^*) = D_{\mathrm{P}}^{\mathrm{ff}}(\mathbf{q}^*)/D^0$ and $D_{\mathrm{P}}^{\mathrm{fw}*}(\mathbf{q}^*) = D_{\mathrm{P}}^{\mathrm{fw}}(\mathbf{q}^*)/D^0$ where $D^0 = 3/2\sqrt{(\pi/\beta m)}\sigma_{\mathrm{w}}$. Thus,

$$D_{\mathrm{P}}^{\mathrm{ff}*}(\mathbf{q}^*) = \frac{\sigma_{\mathrm{w}}^2}{\sigma^2\int \mathrm{d}\hat{\sigma} n^*(\mathbf{q}^*-(\sigma/\sigma_{\mathrm{w}})\hat{\boldsymbol{\sigma}})g(\mathbf{q}^*,\mathbf{q}^*-(\sigma/\sigma_{\mathrm{w}})\hat{\boldsymbol{\sigma}})} \tag{10}$$

and

$$D_{\mathrm{P}}^{\mathrm{fw}*}(\mathbf{q}^*) = \frac{\sigma_{\mathrm{w}}^2}{\sqrt{2}\sigma_{\mathrm{fw}}^2\int \mathrm{d}\hat{\boldsymbol{\sigma}}\, n_{\mathrm{w}}^*(\mathbf{q}^*-(\sigma_{\mathrm{fw}}/\sigma_{\mathrm{w}})\hat{\boldsymbol{\sigma}})\, g_{\mathrm{fw}}(\mathbf{q}^*,\mathbf{q}^*-(\sigma_{\mathrm{fw}}/\sigma_{\mathrm{w}})\hat{\boldsymbol{\sigma}}\,)} \tag{11}$$

Of course, Eq. (9) holds for the dimensionless diffusion coefficients as well.

2.2. Molecular dynamics simulation techniques

The contact values of the equilibrium PCF's which feature in the PG-theoretical expressions can be determined from the integral equations of equilibrium statistical mechanics as applied to nanofluids, or using the EMD technique. The former is the more general and sophisticated approach, but it involves the development of accurate methods for specification, reduction and solution of the complicated integral equation problem. While we believe that such a method will be available in the near future, we use here the EMD technique to simplify our task in evaluation of the zero-order approximation of the PG-theoretical self-diffusion coefficient specific to the

pore fluid of interest. The EMD algorithm is analogous to the procedure employed in the NEMD computations with the exception that in the case of EMD we consider the pure fluid strictly at equilibrium and for this reason we restrict our description of the simulation techniques employed here to the NEMD procedure alone.

The NEMD simulation of structureless Lennard–Jones particles confined within the model pore structure illustrated in Fig. 1 follows the basic principles described in detail in earlier work ([8,14,15,38], see also [7,9,13,22,27,39]). The specific details appropriate to the study undertaken here are summarised below.

The pore structure shown in Fig. 1 is a simplified model of a nanoporous crystal containing a central octahedral cage and two square channels on either side of this cavity. The centre of the Cartesian coordinate system is in the centre of the pore with the z-axis running along the pore and the x- and y-axes orthogonal to the pore walls of the square channels. The axial half length, L, of the composite pore was $L_s + 2.5\sqrt{2}$ and four square channel lengths $L_s = 3.5\sqrt{2}$, $5.5\sqrt{2}$ $7.5\sqrt{2}$ and $9.5\sqrt{2}$ were investigated in the simulations (we note that EMD simulations for the PCFs of PG-theory were conducted only for the case $L_s = 3.5\sqrt{2}$). The walls of the octahedron (maximum dimension $d_0 = 8\sqrt{2}$) and the square channels (width $d_s = 3\sqrt{2}$) are composed of two dense face-centred cubic layers of stationary atoms. The bulk regions to the left and right of the pore structure are bounded by confining walls at $L_3 = \pm(18.5\sqrt{2} + L_s)$ (see Fig. 1(a)), and in both regions control volumes exist (volumes I in the range $-L_2 < z < -L_1$ and II in the range $L_1 < z < L_2$ where $L_1 = (10.5\sqrt{2} + L_s - 5/3)$ and $L_2 = L_1 + 5/3$) within which the chemical potentials of the components in the fluid mixture are maintained constant during the course of the simulations. In all the simulations, the fluid particles interact with each other and with the atoms of the pore structure via the shifted force form of the Lennard–Jones 12-6 potential

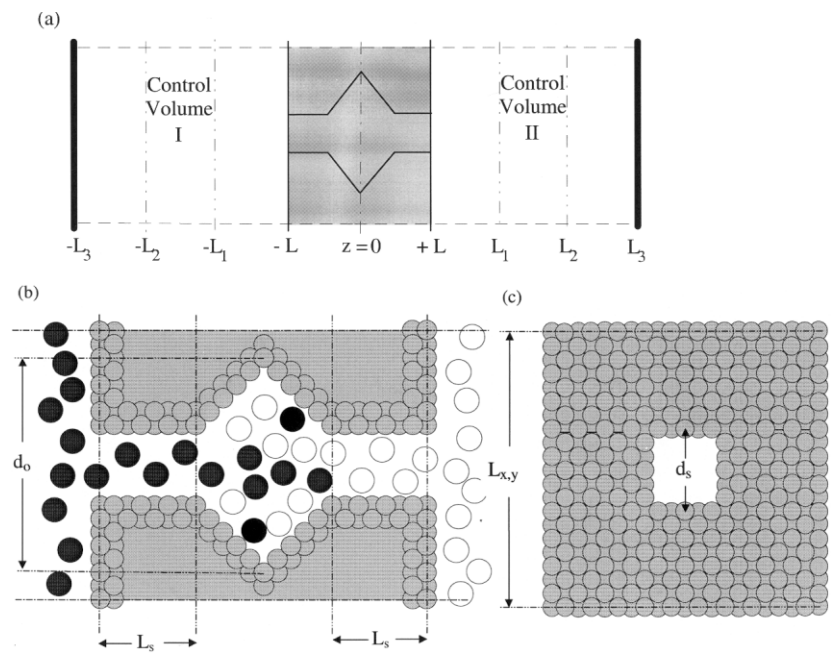

Fig. 1. Model system for nonequilibrium MD simulations. (a) The fundamental cell (imaged in the x and y directions) with control volumes I and II; (b) side view of the nanopore structure employed in the central region of (a); (c) pore face. (Figures (b) and (c) are drawn to scale).

Table 1
Lennard–Jones potential parameters

Component pair	σ (nm)	ε/k (K)
CH_4–CH_4	0.3817	148.2
O–O[a]	0.3	228.4
CH_4–O	0.3409	184

[a] The oxygen atoms are designated as the wall component (w) in the body of the text.

$$\phi_{ij}^{SF}(r_{ij}) = \phi_{ij}(r_{ij}) - \phi_{ij}(r_{cut}) - \left(\frac{d\phi_{ij}(r_{ij})}{dr_{ij}}\right)_{r_{cut}} (r_{ij} - r_{cut}) \quad r_{ij} \le r_{cut}$$
$$= 0 \quad r_{ij} > r_{cut} \tag{12}$$

with

$$\phi_{ij}(r_{ij}) = 4\varepsilon_{ij}\left(\left(\frac{\sigma_{ij}}{r_{ij}}\right)^{12} - \left(\frac{\sigma_{ij}}{r_{ij}}\right)^{6}\right)$$

where r_{cut} is the cut-off distance, $2.5\sigma_{ij}$, and σ_{ij} and ε_{ij} are the codiameter and potential well depth for particles i and j, respectively. The potential parameters employed in this work (methane-like fluid and oxygen wall atoms) are summarised in Table 1.

To initiate a given simulation, the upstream and downstream chemical potentials, μ_i^{I} and μ_i^{II}, respectively, of the counterdiffusing species are selected, and the grand canonical Monte Carlo (GCMC) algorithm proposed by Adams [40] is employed to accumulate fluid particles in the accessible volume in the range $z < 0$ (μ_i^{I}) and in the range $z > 0$ (μ_i^{II}). Typically, 10^5 GCMC events (insertion or deletion of a particle followed by a particle move) were conducted in these computations and the chemical potentials were selected so that the bulk density of the fluid on either side of the fundamental cell was $n^* = 0.5$ in units of the inverse cube of the fluid particle size σ. To complete the initialisation stage of the simulation (including the approach to steady state) particle velocities are assigned from the Maxwell–Boltzmann distribution function at the specified temperature ($T^* = kT/\varepsilon = 1.5$ in all of the simulations reported in this work) and the particle trajectories are computed by solving Newton's equations of motion using Gear's fifth order predictor-corrector [41] with a time step of 0.0035τ where $\tau = \sigma\sqrt{m/\varepsilon}$ ($= 1.376$ ps for the methane-like fluid employed here). During the approach to steady-state velocity rescaling was employed to maintain the system at the desired temperature, however, once steady-state had been reached, the particle dynamics were thereafter strictly computed at fixed energy. Furthermore, in the approach to steady-state, as well as in the steady-state production phase of the computations, GCMC control of the chemical potentials of the species in the mixture is employed only within the two volumes I and II. The individual values of μ_i^{I} and μ_i^{II} are maintained constant by conducting 250 trial insertions and deletions in each control volume at every tenth time step in the MD computations. Steady-state conditions were generally achieved using this GCMC control in association with NVE MD computation of the fluid particle trajectories after a period of 0.5×10^6–2×10^6 time steps. Production runs at steady state were then conducted for up to 5×10^6 additional time steps.

As noted above, Gear's fifth order predictor-corrector was used to compute the trajectories. However, one modification was introduced to efficiently restart the particle trajectories after each GCMC control stage in the simulations. Each time, the control volumes were reconfigured (every ten time steps) the 3rd and 4th (as well as the 2nd) order terms in the expansion for the prediction step (and the corresponding terms in the expansions for $\mathbf{v}(t+\delta t)$, $\mathbf{a}(t+\delta t)$, $\mathbf{b}(t+\delta t)$ and $\mathbf{c}(t+\delta t)$)

$$\mathbf{q}(t+\delta t) = \mathbf{q}(t) + \delta t\,\mathbf{v}(t) + \frac{1}{2}\delta t^2\mathbf{a}(t) + \frac{1}{6}\delta t^3\,\mathbf{b}(t) + \frac{1}{24}\delta t^4\,\mathbf{c}(t) + \frac{1}{120}\delta t^5\,\mathbf{d}(t)$$

were computed analytically for each particle in the system. While this incurs an additional time cost in the calculations it was actually found that the computational speed was only reduced by approximately 10% while ensuring excellent energy conservation during the NVE phase of the simulation. Computing $\mathbf{d}(t)$ analytically, however, was not undertaken (this value was restarted as $\mathbf{0}$) because this required a greater degree of computa-

tional time with only a minor improvement in energy conservation.

The steady-state fluxes are determined by monitoring the net transfer of particles across one or more planes within the system. The steady-state flux in the z-direction is computed using

$$J_i^z = \frac{1}{L_x L_y} \frac{(N_i^+ - N_i^-)}{\Delta t \, N_p} \quad (13)$$

where N_i^+ and N_i^- are the total number of particles of component i which have drifted downstream (in the direction of net flow) and upstream (counter to the direction of net flow), respectively, normal to a total number of N_p planes of cross-section $L_x L_y = 200$ (in units of σ_w^2) during an observation time Δt. In this work $N_p = 3$ and the planes were located at $z = -L$, 0 and $+L$.

In addition to providing particle fluxes, the nonequilibrium simulations will also give full details of the species concentration profiles from which one may either determine global permeabilities or local transport coefficients. The former are easily defined by

$$P_i = \frac{J_i^z}{(n_{B,i}^I - n_{B,i}^{II})} \quad (14)$$

where $n_{B,i}^k$ is the concentration of component i in control volume k (k = I or II). The manner in which the local transport coefficients are determined from the NEMD results will be described later in Section 3.2.

3. Results and discussion

3.1. EMD simulations

The local values of the equilibrium fluid number density and the fluid–fluid and fluid–wall PCF contact values that are required to calculate the theoretical values of the tracer self-diffusion coefficient in the zero-order approximation, Eq. (1), have been simulated using a rather straightforward 3-dimensional generalisation of the method described in [35,36]. The data obtained have been used to calculate, $D_P^{ff*}(\mathbf{q}^*)$, $D_P^{fw*}(\mathbf{q}^*)$, $D_P^*(\mathbf{q}^*)$, their across-the-pore average values specific to each of the z-bins, $D_P^{ff*}(z^*)$, $D_P^{fw*}(z^*)$, $D_P^*(z^*)$, respectively, and

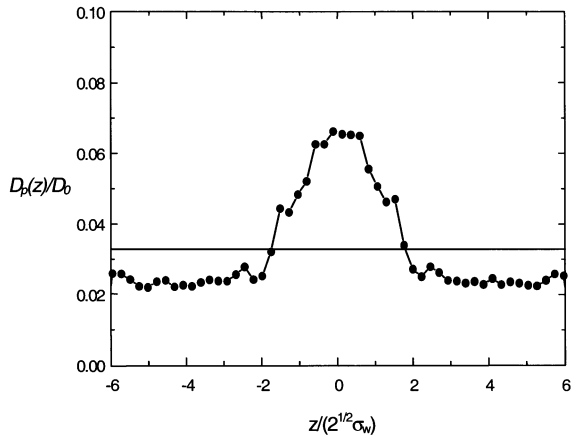

Fig. 2. Zero-order approximation for the across-the-pore average of the PG-theoretical self-diffusion coefficient for the pore system. The horizontal line corresponds to the overall average value of the theoretical self-diffusion coefficient.

the total average D_P^* values for the square channels, the octahedral cavity and the entire pore. These results are illustrated in Figs. 2–9. Due to restrictions on available computational resources which did not permit extra 'fine' division of the pore space into bins for the memory demanding requirements involved in the calculation of the PCF contact values, the entire pore system was divided into $30 \times 30 \times 60$ bins in the x-, y- and z-directions, respectively, where the z-axis coincides with the axis of the pore system (Fig. 2). Therefore, the PCF

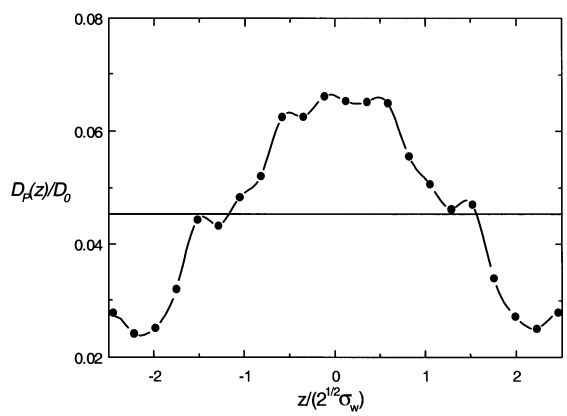

Fig. 3. Zero-order approximation for the across-the-pore average of the PG-theoretical self-diffusion coefficient for octahedron cavity. The horizontal line corresponds to the average value of the theoretical self-diffusion coefficient.

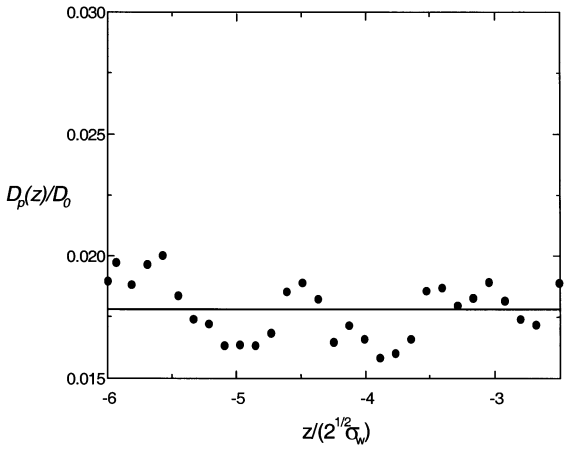

Fig. 4. Zero-order approximation for the across-the-pore average of the PG-theoretical self-diffusion coefficient for the square channel. The horizontal line corresponds to the pore averaged theoretical diffusion coefficient.

contact values obtained for the entire system (including the central octahedron unit (Fig. 3)) were computed rather 'coarsely'. To simulate the contact PCF values more accurately (at least for part of the system), we also divided one of the square channels into much finer bins, again dividing its space into $30 \times 30 \times 45$ bins in the x-, y- and z-directions. The contact values of the PCFs so obtained lead to much better agreement between the theoretical and NEMD values of the average diffusion coefficient for the channel than for the central unit (see Figs. 4, 5 and 9) as may be observed from the results summarised in Table 2. The magnitudes of the individual fluid and wall terms in the self-diffusivity which are reported in Fig. 5(b) also confirm an intuitive expectation that the direct contribution to the self-diffusion coefficient of the pore nanofluid due to the fluid–wall intermolecular interactions within the very narrow channel are largely responsible for the significant decrease in the value of the self-diffusion coefficient relative to the bulk. The average number density of the confined 'methane' nanofluid in fluid σ-units, $n_f^* = n\sigma^3$, is 0.40 ± 0.04 (it is noteworthy that bulk methane at this density and temperature possesses a pressure of about 220 atm [42]) and the self-diffusion coefficient for the model methane Lennard–Jones fluid in the bulk state has been independently determined using traditional EMD procedures [43] to be 3.4×10^{-4} $cm^2\ s^{-1}$. The average zero-order theoretical value of the nanofluid self-diffusion coefficient specific to the entire pore is 0.894×10^{-4} $cm^2\ s^{-1}$ (second row of Table 2), which is four times smaller than its bulk fluid value. In the square channels this coefficient drops to 0.483×10^{-4} $cm^2\ s^{-1}$, which is seven times smaller than the corresponding bulk value. Much of this decrease is due to direct fluid–wall intermolecular interactions. The remainder comes from implicit effects of these inter-

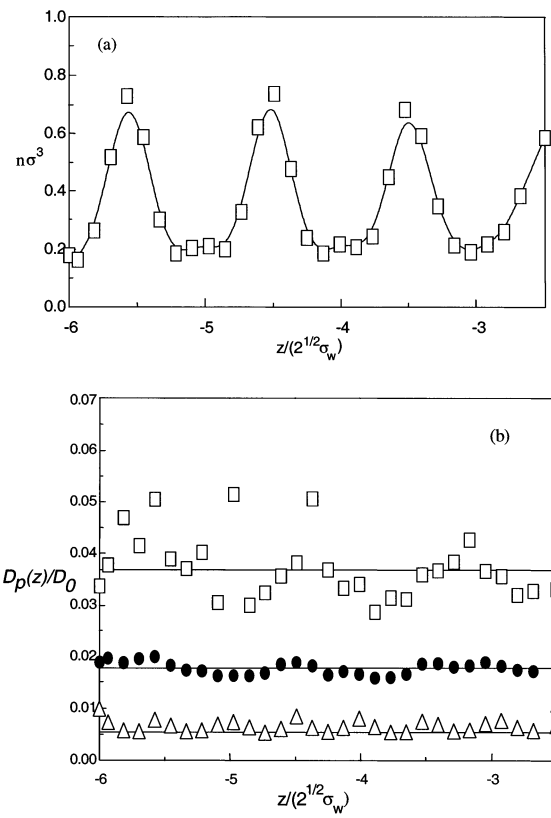

Fig. 5. (a) The open squares represent the average fluid density (based on pore cross-section d_s^2) for z-bins within the left square channel shown in Fig. 1, and the curve corresponds to a fit by B-splines. (b) The fluid–fluid and fluid–wall contributions, D_P^{ff}/D^0 (open squares) and D_P^{fw}/D^0 (open triangles), respectively, to the zero-order approximation of the across-the-pore average of the PG-theoretical self-diffusion coefficient for the square channel. The horizontal lines correspond to the average values which in each case are $< D_P^{ff}/D^0 > = 0.0372$; $< D_P^{fw}/D^0 > = 0.0062$; and overall (the filled circles) $< D_P/D^0 > = 0.0178$.

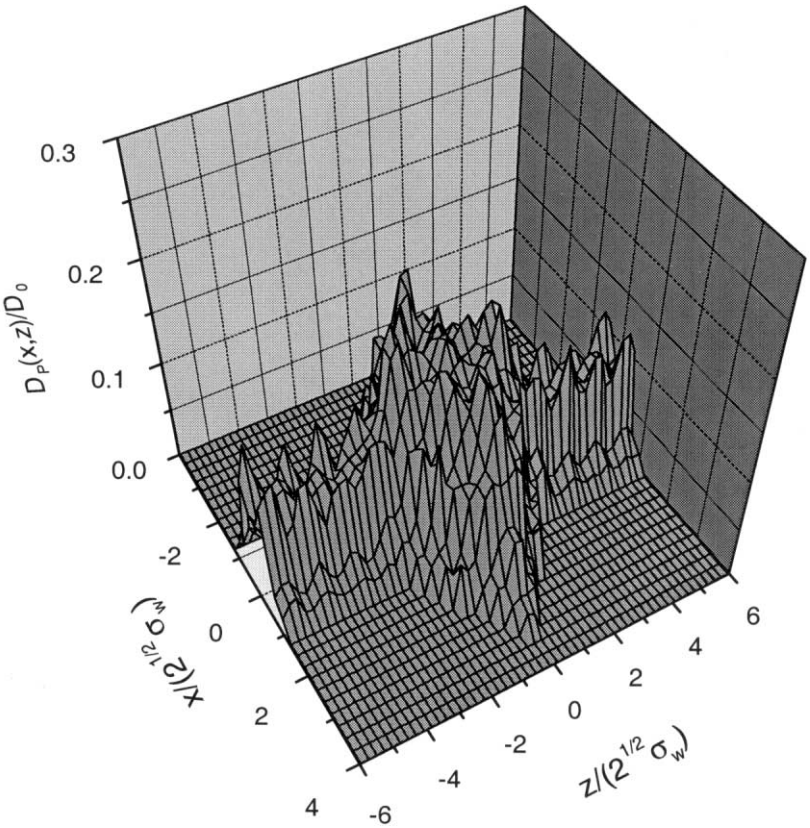

Fig. 6. Zero-order approximation of the PG-theoretical self-diffusion coefficient for the entire pore system in the plane $y = 0$.

actions in-built into the contact values of the pore fluid–fluid PCF and the pore fluid number density. The theoretical self-diffusion data contain an average statistical error of about 20% after 9 million time steps of the EMD simulations. This error emerges primarily from calculations of the contact values of the PCFs (especially the fluid–wall PCFs). This error can be made much smaller provided much smaller bin sizes and much longer EMD simulations runs are adopted. Our computational facilities did not permit such bin refinement or increase in time in these preliminary computations.

3.2. NEMD simulations

To compare the theoretical predictions for the self-diffusion coefficients within the pore employed in the earlier section ($L_s = 3.5\sqrt{2}$) with molecular simulation, we have computed the steady-state particle number flow and the 'species' concentration profiles along the axial direction of the pore using the NEMD technique described earlier. The average value of the particle diffusion flow for this system was found to be 14.1 ± 0.7 fluid particles per nanosecond and the corresponding 'species' concentration profiles are shown in Fig. 10. These profiles are the porous medium cross-section averaged results (area $= L_x L_y$) obtained for individual axial z-bins of width $0.05 \times \sqrt{2}\sigma_w$, and to extract reasonable estimates of the diffusion coefficients the following procedure is employed. The average NEMD values of the self-diffusion coefficients, D_{NEMD}, are found from a correlation similar to Eqs. (4) and (6) which, on averaging over the cross-section, provides

$$\bar{J}^{z}_{1*} = \frac{1}{A}\int J^{z}_{1*}\,\mathrm{d}x\mathrm{d}y = -\left[\frac{\int D_{\mathrm{P}}(\mathbf{q})(\partial\delta n_{1*}(\mathbf{q})/\partial z)\mathrm{d}x\mathrm{d}y}{\int(\partial\delta\, n_{1*}(\mathbf{q})/\partial z)\mathrm{d}x\mathrm{d}y}\right]\frac{1}{A}\int\frac{\partial\delta\, n_{1*}(\mathbf{q})}{\partial z}\,\mathrm{d}x\mathrm{d}y = -\bar{D}_{\mathrm{P}}(z)\,\frac{\partial\delta\,\bar{n}_{1*}(z)}{\partial z} \qquad (15)$$

To qualify the comparison with the averaging conducted on the PG-theoretical results it should be noted that, while the cross-section averaged flow $\bar{J}^{z}_{1*}A$ is independent of z at steady state, this is not necessarily true of either the averaged diffusion coefficient or the gradient of the averaged deviation of the nonequilibrium concentration from its equilibrium local value as defined by Eq. (15). One should also note that the averaged diffusivity defined by the above expression is not precisely the same as the cross-section averaged diffusivity computed from PG theory *unless* the concentration deviation $\delta n_{1*}(\mathbf{q})$ is independent of x and y. The latter is a reasonable assumption for pores with smooth walls without geometric inhomogeneities such as varying pore cross-section in which case the x and y components of the diffusion fluxes J^{x}_{1*} and J^{y}_{1*} should be negligible. However, for pores with atomistically structured walls and/or varying cross-section the deviation of the non-equilibrium fluid density from its equilibrium value exhibits a strong dependence on all the

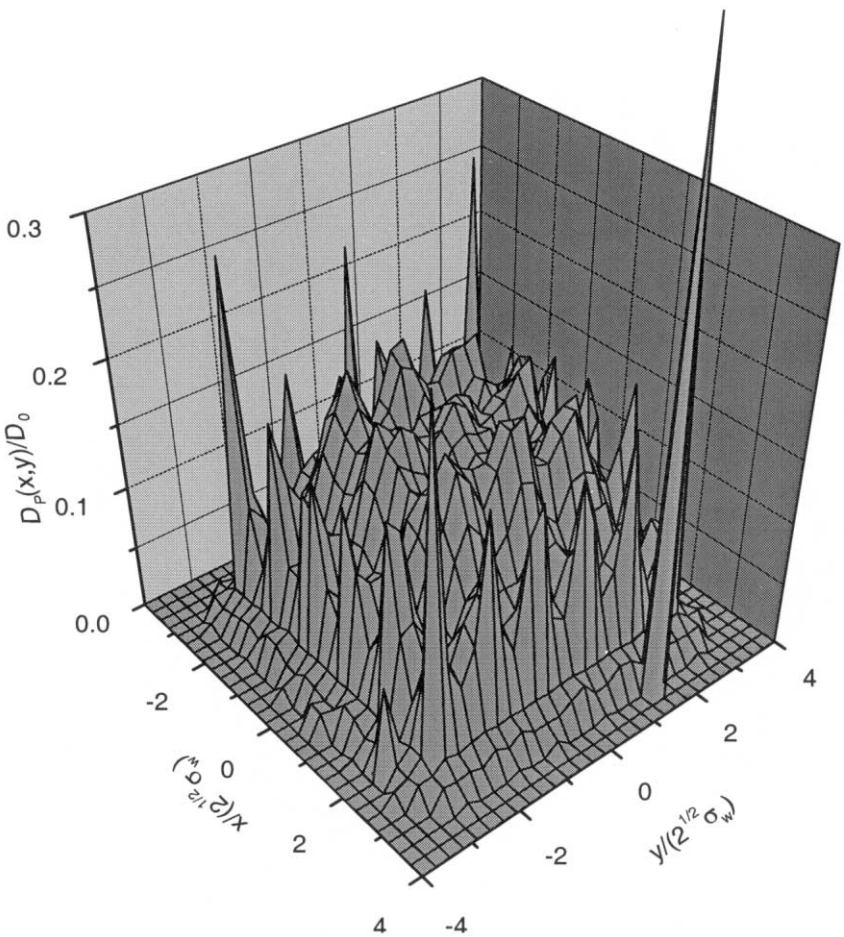

Fig. 7. Zero-order approximation of the PG-theoretical self-diffusion coefficient for the central cross-section of the octahedron cavity at $z = 0$.

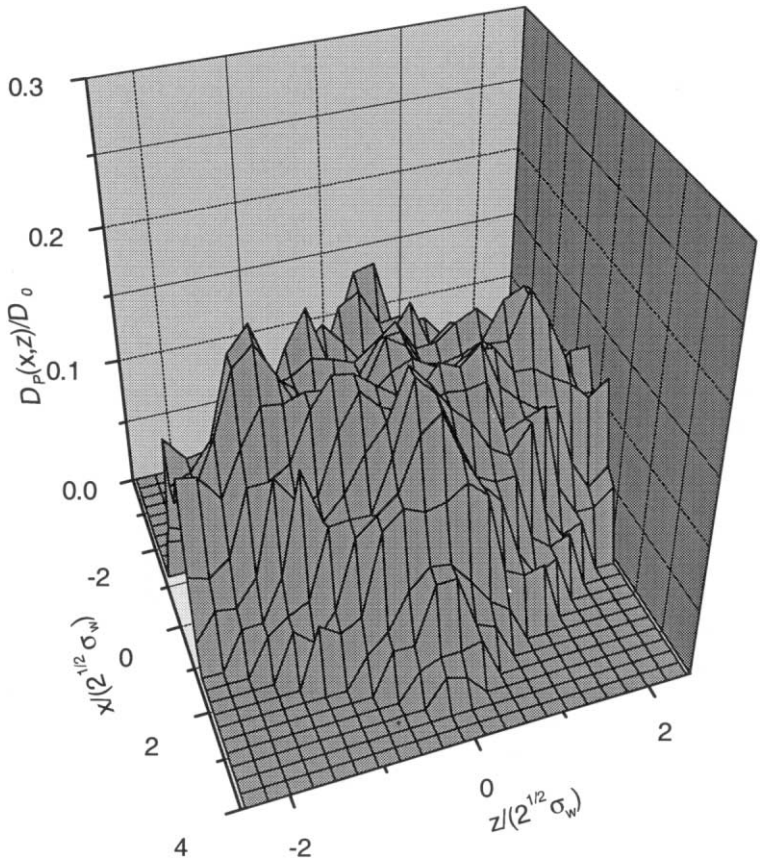

Fig. 8. Zero-order approximation of the PG-theoretical self-diffusion coefficient for the central cross-section of the octahedron cavity at $y = 0$.

coordinates [36,44]. In conjunction with diffusion, this means that the flux components cannot be assumed to be negligible locally.

The concentration deviation $\delta\bar{n}_i(z)$ also introduces a complication into the analysis since in general for the self-diffusing fluid under consideration here we do not have direct access to numerical estimates of the equilibrium local concentrations of both 'species' which appear in this deviation. In principle this problem can be avoided by locally integrating Eq. (15) over z between two axial positions which are isomorphic to one another. However, if this approach is employed, it may be readily shown that the effective diffusivity so obtained depends on the specific isomorphic state selected and this problem can be traced back to the fact that locally both J^x_{1*} and J^y_{1*} are strictly nonzero in the system under consideration in this work. Therefore, it is necessary to introduce a second local averaging over a narrow range of axial bins to, in effect, cancel the negative components of these fluxes with their positive contributions. This averaging is done in such a way that the modified concentration deviations correspond to coarse grained isomorphic states separated by a distance L_{iso} and distributed along the axial direction of the pore. This is equivalent to a local volume averaging of the concentrations in isomorphic states i.e.

$$\frac{1}{L_{\mathrm{iso}}}\int \delta\bar{n}_{1*}(z)\mathrm{d}z = \delta\tilde{n}_{1*} \tag{16}$$

and in view of the cancellation of the equilibrium concentrations between these states we approxi-

mate the gradient in Eq. (15) by $\Delta\tilde{n}_{1*}/\Delta z$ where $\Delta z \equiv L_{iso}$. In all of our calculations of this gradient we have taken L_{iso} to be equal to the lattice spacing, $\sqrt{2}\sigma_w$, of the solid surface. We also note that only the square channel will be examined here (with one exception to be discussed below) since the z-varying cross-section of the octahedral cavity precludes a reliable assessment of the diffusivity by this method without explicit details of the equilibrium local concentrations of the 'species' as functions of x and y, as well as z.

The results of this analysis in the form of the pore averaged diffusivity for the square channels, D_{NEMD}, within the short pore structure are reported in Table 2. The deviation of the theoretical value and the value of the self-diffusion coefficient obtained using the heuristic treatment Eqs. (15) and (16) of the NEMD data is approximately -15%. In view of the approximations inherent in the averaging procedure described above and the fact that the PG theoretical values themselves were calculated in the zero order approximation we can conclude that the results agree exceptionally well.

In Table 2, we also report an estimate for the self-diffusivity within the octahedron. Note that this value deviates more significantly from the PG-theoretical averaged value than does the corresponding value for the square channel and, as noted above, we believe this results from the greater influence of the x–y dependence of the gradients appearing within the averaged diffusivity in Eq. (15). In practice, therefore, we suggest that Eqs. (15) and (16) should not be used for pores with strong geometric inhomogeneities (e.g. the octahedron in the present case or sphere-like cavities in zeolites) unless details of the **q**-dependence of the concentrations are available.

To further assess the possible influence of the nanometer scale inhomogeneities at the entrances and exits of the square channels we have conducted NEMD simulations for three additional

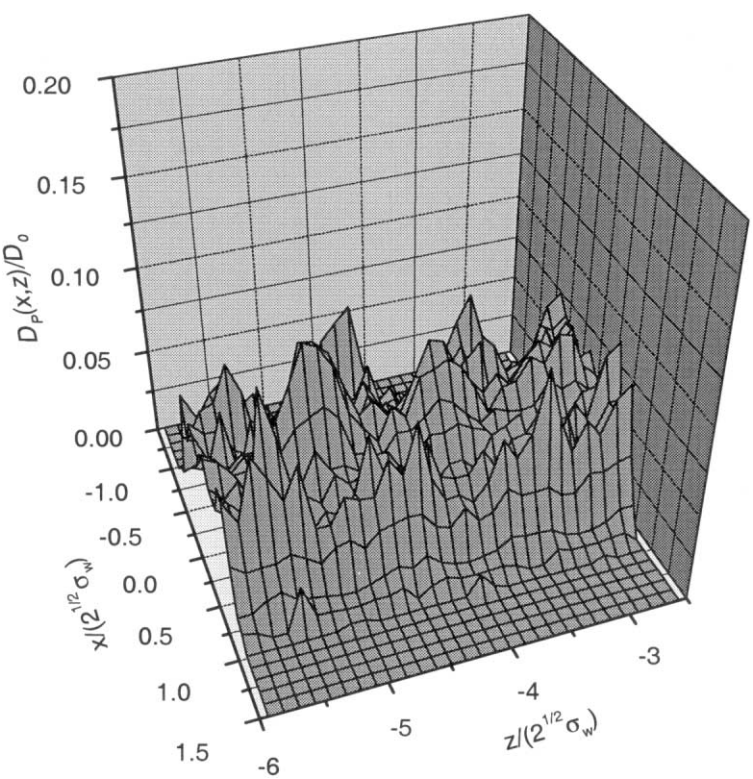

Fig. 9. Zero-order approximation of the PG-theoretical self-diffusion coefficient for the square channel in the plane $y = 0$.

Table 2
The self-diffusion coefficient of the pore nanofluid

Pore section	Square channel	Central octahedron section	Entire pore
Theoretical average value, $D_P \times 10^4$ ($cm^2\ s^{-1}$)	0.483	1.232	0.894
NEMD value using Eqs. (15) and (16), $D_{NEMD} \times 10^4$ ($cm^2\ s^{-1}$)	0.57	0.76	–
$(D_P - D_{NEMD}/D_{NEMD}) \times 100\%$	−15.2	62.1	–

pores containing square channels of the same width but of different length. The overall system permeability obtained using Eq. (14) is plotted as a function of the sum of the two square channels lengths in Fig. 11, and while it would appear that the simple linear formula

$$\frac{1}{P} = \frac{1}{P_0} + \frac{2L_s}{D_{app}} \tag{17}$$

fits the results, this is deceptive and indeed incorrect, particularly for the shorter pores. A clear indication of this is the *negative* intercept, which the simplified correlation provides. A closer analysis of the NEMD concentration profiles using the method described above with reference to Eqs. (15) and (16) provides the coarse grained diffusion coefficients shown in Fig. 12. It is clear from the results for the three longer square channel pores that the pore mouth connecting the bulk fluid or the octahedral cavity to the square channels on the upstream side of these channels significantly influences the apparent magnitude of the self-diffusivity over a square channel length scale commensurate with the actual length of the shortest pore ($L_s = 3.5\sqrt{2\sigma_w}$). For the longer pores, however, the results suggest that an interior square channel diffusivity of approximately 0.45×10^{-4} $cm^2\ s^{-1}$ is obtained for both channels. We emphasise that this result cannot be readily obtained from Eq. (17) and it is only on the basis of guidelines implicit in PG theory (notably diffusion forces proportional to gradients of the concentration *deviations*) coupled with details of the nonequilibrium profiles that such an analysis can be carried out.

4. Conclusions

The self-diffusivity of a Lennard–Jones fluid in a model crystalline nanopore as calculated to zero order in the rigorous statistical mechanical theory of Pozhar and Gubbins [1,2] and results obtained from NEMD simulations processed via Eqs. (15) and (16) have been shown to agree to within −15–63%. Due to the heuristic nature of the analysis of the NEMD data to obtain the final results, and also the zero-order approximation to the theoretical self-diffusion coefficient, the numbers reported here should be viewed as qualitative estimates rather than definitive values for the nanofluid diffusion coefficients within the system

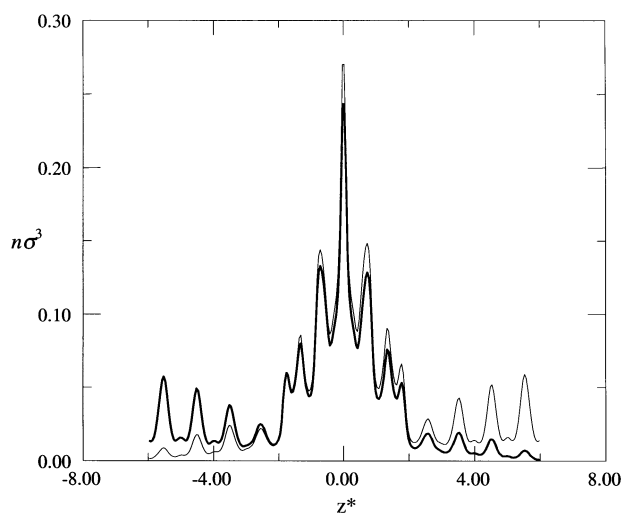

Fig. 10. The non-equilibrium density profile of the counterdiffusing components expressed in the units of σ^3 specific to the fluid atomic diameter. z^* is in units of $\sqrt{2\sigma_w}$.

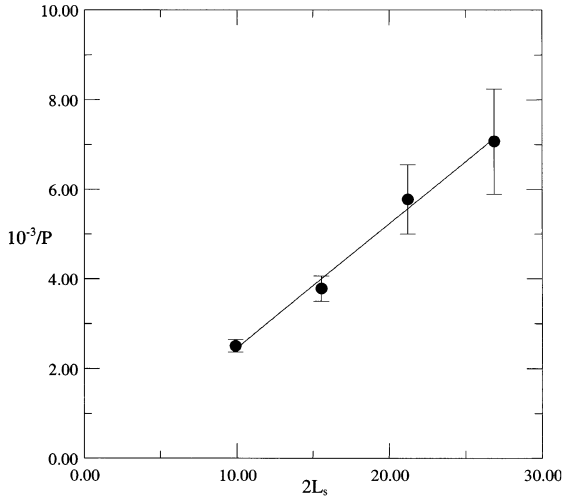

Fig. 11. The inverse permeability P (in units of σ_w/τ) as a function of the overall length $2L_s$ (in units of σ_w) of both square channels.

considered. It is also clear from the results that an approximate analysis of NEMD data based on a spatially averaged, one-dimensional correlation between the local particle flux and the local concentration gradient analogous to bulk fluids is unlikely to be applicable to strongly inhomogeneous fluids and, in general, extreme care should be exercised when attempting to interpret local transport behaviour from coarse-grained data.

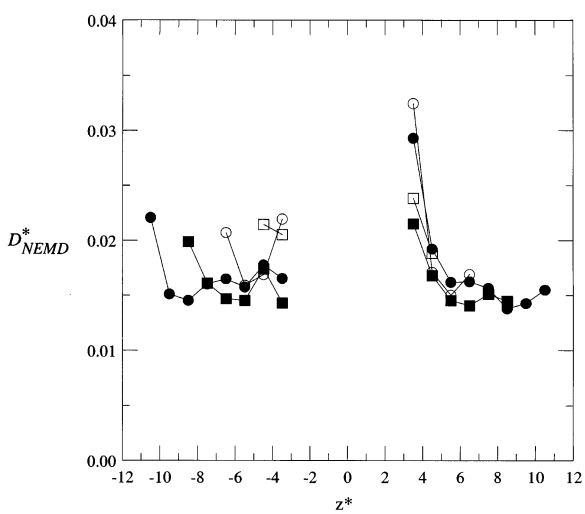

Fig. 12. The coarse-grained NEMD diffusion coefficient within the square channels as a function of axial position. D^*_{NEMD} is in units of D^0 and z^* is in units of $\sqrt{2}\times\sigma_w$. □ $L_s = 3.5\sqrt{2}$; ○ $L_s = 5.5\sqrt{2}$; ■ $L_s = 7.5\sqrt{2}$; ● $L_s = 9.5\sqrt{2}$ (with L_s in units of σ_w).

A fundamental problem, which we believe contributes to the necessity for introducing the averaging involved in Eqs. (15) and (16), is that the nanofluid transport coefficients are non-local, as demonstrated extensively by PG-theoretical analysis and recent MD simulations [36,44]. To describe the system evolution in terms of coarse-grained data one would need to develop a theoretical description of the physical mechanisms that are responsible for the emergence of the collective modes of many-particle systems from the chaotic thermal movement of the particles, and this is exactly the major task of rigorous statistical mechanical theory. PG theory provides a rigorous framework together with general results on the transport coefficients and, as demonstrated in this work, offers a number of possibilities for simplification of the theoretical expression(s), in particular for the diffusion coefficients of nanofluids, for practical use in engineering design. While further work is still required to specify particular engineering models, it is apparent that a fundamental problem, namely the interrelationship of the microscopic dynamics and the atomistic and geometric structure of the nanopore system, now has a tractable solution.

Acknowledgements

LAP is grateful to the Engineering and Physical Sciences Research Council (UK) for support of this work and JMDM wishes to acknowledge partial support from INTAS Project 96-1186.

References

[1] L.A. Pozhar, K.E. Gubbins, J. Chem. Phys. 99 (1993) 8970.
[2] L.A. Pozhar, K.E. Gubbins, Phys. Rev. E56 (1997) 5367.
[3] J.J. Magda, M. Tirrell, H.T. Davis, J. Chem. Phys. 83 (1985) 1888.
[4] S.-H. Suh, J.M.D. MacElroy, Mol. Phys. 58 (1986) 445.
[5] J.M.D. MacElroy, S.-H. Suh, Mol. Phys. 60 (1987) 475.
[6] J.M.D. MacElroy, S.-H. Suh, Molec. Sim. 2 (1989) 313.

[7] R.F. Cracknell, D. Nicholson, N. Quirke, Phys. Rev. Lett. 74 (1995) 2463.
[8] J.M.D. MacElroy, S.-H. Suh, J. Chem. Phys. 106 (1997) 8595.
[9] L.F. Xu, M.G. Sedigh, M. Sahimi, T.T. Tsotsis, Phys. Rev. Lett. 80 (1998) 3511.
[10] J.M.D. MacElroy, K. Raghavan, J. Chem. Phys. 93 (1990) 2068.
[11] J.M.D. MacElroy, K. Raghavan, J. Chem. Soc. Faraday Trans. 87 (1991) 1971.
[12] P.I. Pohl, G.S. Heffelfinger, J. Membr. Sci. 155 (1999) 1.
[13] S. Furukawa, T. Shigeta, T. Nitta, J. Chem. Eng. Jpn. 29 (1996) 725.
[14] J.M.D. MacElroy, N.A. Seaton, S.P. Friedman, Chem. Eng. Sci. 54 (1999) 1015.
[15] J.M.D. MacElroy, M.J. Boyle, Chem. Eng. J. 74 (1999) 85.
[16] L.F. Xu, T.T. Tsotsis, M. Sahimi, J. Chem. Phys. 111 (1999) 3252.
[17] F. Muller-Plathe, S.C. Rogers, W.F. van Gunsteren, Chem. Phys. Lett. 199 (1992) 237.
[18] A.A. Gusev, S. Arizzi, U.W. Suter, D.J. Moll, J. Chem. Phys. 99 (1993) 2221.
[19] F. Muller-Plathe, J. Chem. Phys. 103 (1995) 4346.
[20] P. Neogi, Diffusion in Polymers, Marcel Dekker, New York, 1996.
[21] S. Sunderrajan, C.K. Hall, B.D. Freeman, J. Chem. Phys. 105 (1996) 1621.
[22] D.M. Ford, G.S. Heffelfinger, Mol. Phys. 94 (1998) 673.
[23] D.A. Mooney, J.M.D. MacElroy, J. Chem. Phys. 110 (1999) 11087.
[24] E.J. Maginn, A.T. Bell, D.N. Theodorou, J. Phys. Chem. 97 (1993) 4173.
[25] R. Haberlandt, J. Kärger, Chem. Eng. J. 74 (1999) 15.
[26] K. Hahn, J. Kärger, J. Phys. Chem. 100 (1996) 316.
[27] P.I. Pohl, G.S. Heffelfinger, D.M. Smith, Mol. Phys. 89 (1996) 1725.
[28] J.N. Israelachvili, P.M. McGuiggan, A.M. Homola, Science 240 (1988) 189.
[29] J. van Alsten, S. Granick, Phys. Rev. Lett. 61 (1998) 2570.
[30] S. Granick, Science 253 (1991) 1374.
[31] S. Sarman, D.J. Evans, P.T. Cummings, Phys. Rep. 305 (1998) 1.
[32] I. Bitsanis, T.K. Vanderlick, M. Tirrell, H.T. Davis, J. Chem. Phys. 89 (1988) 3152.
[33] H.T. Davis, J. Chem. Phys. 86 (1987) 1474.
[34] H.T. Davis, Chem. Eng. Commun. 58 (1987) 413.
[35] L.A. Pozhar, Proc.Y2K International Conference on Dynamical Systems and Differential Equations, 18–21 May 2000, Kennesaw, GA (in press).
[36] L.A. Pozhar, Phys. Rev. E61 (2000) 1432.
[37] E. Akhmatskaya, B.D. Todd, P.J. Daivis, D.J. Evans, K.E. Gubbins, L.A. Pozhar, J. Chem. Phys. 106 (1997) 4684.
[38] J.M.D. MacElroy, J. Chem. Phys. 101 (1994) 5274.
[39] G.S. Heffelfinger, F. van Swol, J. Chem. Phys. 100 (1994) 7548.
[40] D.J. Adams, Mol. Phys. 29 (1975) 307.
[41] C.W. Gear, Numerical Initial Value Problems in Ordinary Differential Equations, Englewood Cliffs, NJ 1971.
[42] J.O. Hirschfelder, C.F. Curtiss, R.B. Bird, Molecular Theory of Gases and Liquids, Wiley, New York, 1954.
[43] M.P. Allen, D.J. Tildesley, Computer Simulation of Liquids, Clarendon, Oxford, 1987.
[44] K.P. Travis, B.D. Todd, D.J. Evans, Physics A240 (1997) 315.